Table 1. Comparison of TRMM-derived geolocation with IMD and JTWC best-track positions for four specific cases

Date	Time (UTC)	TRMM-derived geolocation (lat/long)	IMD best-track position interpolated to TRMM overflight time	JTWC best-track position interpolated to TRMM overflight time	Difference (km) TRMM–IMD	Difference (km) TRMM–JTWC	Difference (km) IMD–JTWC
21-11-98	00 : 57	17.31N 87.68E	16.66N 87.50E	16.94N 87.54E	62.9	41.8	31.3
18-05-99	13 : 47	19.05N 67.14E	18.50N 67.50E	19.11N 67.27E	71.8	15.2	71.9
26-10-99	16 : 33	15.57N 93.05E	15.00N 93.66E	15.45N 93.29E	90.9	28.9	63.7
27-10-99	00 : 39	16.14N 92.19E	15.61N 91.78E	16.04N 92.21E	71.8	10.5	66.2

tures of satellite-derived positions from JTWC best-track positions are quite small compared to those from IMD best-track positions. In a recent study, Ahn *et al.*[12] also noticed that the best-track position determined by regional centres that probably do not use high resolution microwave observations, show significant departures from JTWC best-track positions as well as from TMI-derived geolocation.

Data from 85 GHz channel of TMI have been analysed for several tropical cyclones over the Indian Ocean. 85 GHz images show useful patterns that can be applied for the determination of the centre of the tropical cyclones. Such patterns are not always apparent in visible/infrared images because of the cirrus shield that generally obscures the inner core of the cyclones. A comparison of 85 GHz-based geolocation with the best-track positions available from operational agencies shows that except for a few cases, the difference between the two is significant considering the impact of initial position errors on subsequent predictions (Figure 1). An error analysis based on a large data-set consisting of best-track positions of the Indian Ocean tropical cyclones during past 30 years indicates that such large differences in cyclone geolocation could not have resulted merely from the error of interpolation. These differences are quite significant even after the maximum error due interpolation is taken into account.

1. Elsberry, R. L., Recent advancements in dynamical tropical cyclone track predictions. Meteorology and atmosphereic physics. *Meteorol. Atmos. Phys.*, 1995, **56**, 81–99.
2. Pal, P. K., Cyclone track prediction over the north Indian ocean. *Mon. Weather Rev.*, 1991, **119**, 3095–3098.
3. McBride, J. L. and Holland, G. J., Tropical cyclone forecasting: A world-wide summary of techniques and verification statistics. *Bull. Am. Meteorol. Soc.*, 1987, **68**, 1230–1238.
4. Dvorak, V. F., Tropical cyclone intensity analysis using satellite data. *NOAA Tech. Rep. NESDIS*, 1984, **11**, 47.
5. Rao, B. M., Kishtawal, C. M., Pal, P. K. and Narayanan, M. S., Observations of a Bay of Bengal tropical cyclone from ERS-1 scatterometer. *Int. J. Remote Sensing*, 1995, **16**, 351–357.
6. Velden, C. S., Olson, W. S. and Roth, B. A., Tropical cyclone center-fixing using DMSP SSM/I data. Preprints. Proc. Fourth Conf. on Satellite Meteorology and Oceanography, San Diego, Am. Meteorol. Soc., 1989, pp. J36–J39.
7. Sandlin, G. D. and Spangler, D. J., Naval Research Laboratory Report (Available from Sandlin, G. D., Naval Research Laboratory, Washington DC 20375), 1989, p. 18.
8. Rappaport, E. L., Proc. 19th Conf. on Hurricanes and Tropical Meteorology, Miami, Am. Meteorol. Soc., 1991, pp. 179–183.
9. Randall, J. A., Sethu Raman and Chang, S. W., Special sensor/imager (SSM/I) observations of hurricane Hugo (1989). *Mon. Weather Rev.*, 1992, 2723–2737.
10. Elsberry, R. L., *Tropical Cyclone Motion*, Office of Naval Research, 1987, pp. 91–131.
11. IMD, Reports on cyclonic disturbances over North Indian Ocean, 1998–2001.
12. Ahn, M-H., Seo, Y.-K., Park, H.-S. and Suh, A.-S., Determination of tropical cyclone center using TRMM microwave imager data. *Geophys. Res. Lett.*, 2002, **29**, 15/1–15/4.

Received 19 September 2003; revised accepted 12 April 2004

Fluvial influx and weathering history of the Himalayas since Last Glacial Maxima – isotopic, sedimentological and magnetic records from the Bay of Bengal

Onkar S. Chauhan[1,*], Shiva K. Patil[2] and J. Suneethi[1]

[1]National Institute of Oceanography, Dona Paula, Goa 403 004, India
[2]Indian Institute of Geomagnetism, New Panvel, Mumbai 410 218, India

From temporal variations in stable isotopes, mineral magnetism, clay minerals and granulometric parameters from a ^{14}C dated core have been used to understand weathering history and influence of climate on the terrigenous fluxes into the Bay of Bengal. We deduced well defined events of reduced fluvial influx at 20–15, 12.7, 9.5, ~5–4.3 and 1.8–2.2 Ka BP and at least two major fluvial pulses initiated around 11.5 and 9.5 Ka BP. The intensified monsoon regime appeared to have set in at around 9.5 Ka, and had pauses at ~5 and 2.2 Ka BP during the Holocene.

The climate variability appeared to have significant control over characteristics of terrigenous flux into the bay, particularly during the glaciation events. Illite, chlorite, smectite and kaolinite are the clays present in the core. From the abundance of chlorite (the clays produced in arid cold climate) and increased contents of silt, a reduced chemical weathering during

---

*For correspondence. (e-mail: onkar@darya.nio.org)

events of glaciations has been inferred. Occurrence of coarser magnetic grains in the lower levels of the cores (35–100 cm), perhaps, suggests higher magnitude of physical weathering in Pre-Holocene in the Hinterland. An intensified chemical weathering in the Himalayas, under an active summer monsoon regime after 9.5 Ka BP, appears to have enhanced fluxes of finer magnetic minerals, clay size detritus and reduced chlorite during the entire Holocene (0–30 cm levels).

THE Himalayas are mountains ranges in which weathering intensity is one of the highest in the world. It is also, since Miocene, a major source of the sediment for the Bay of Bengal through a large number of perennial rivers, the Ganga, Brahmaputra, Irrawadi, Salveen, etc. turning it into one of the highest fluvial and terrigenous input sites of the world oceans[1]. The climate of the Indian subcontinent is regulated by coupled heating–cooling of the Himalayas and the Southern Ocean, and associated changes in wind patterns giving rise to the northeast (NE) and the southwest (SW) monsoons[2–4]. Under modern climatology, about 80% of the rainfall is contributed during the SW monsoon. Past studies have, however, suggested a stronger NE monsoon during glaciation of Himalayas[3]. The climatic changes in the region, therefore, are expected to have influences on weathering intensity in the Himalayas and the characteristics and supply of fluvial fluxes into the bay. However, studies and understanding of climate-induced variations in the fluvial flux to ocean and weathering intensity at the Himalayas under specific climatologies of active and weak monsoon regimes are still in the state of infancy.

Sea surface salinity (SSS), in response to fluvial flux undergoes large seasonal variations (~ 7‰ during peak discharge during the SW monsoon[5]; Figure 1) in the bay. A core, from among scores of cores collected during different cruises of ORV *Sagar Kanya*, is selected from a location where under the modern hydrography, SSS is influenced largely by the fluvial discharge of the Ganga–Brahmaputra (G–B) system[5] (Figure 1), and by and large, is a depocentre of terrigenous influx of the Himalayan rivers[6,7]. Because the SSS variations in this area are regulated by the fluvial influx from the Himalayas, d^{18}O of the planktonic foraminifers (which mostly sustain in the upper mixed layer, and their shell secretion is influenced by local SSS and SST changes[8]), archive the variations in the magnitude of climate-induced fluvial flux of the G–B into this region. The d^{18}O variations in these two surface-dwelling planktonic species, therefore, are basis of determining prevalent magnitude of fluvial influx from the G–B. Integrated results of magnetic susceptibility data coupled with granulometric and clay mineralogy are used for reconstructing weathering intensity *vis-à-vis* terrigenous influx under prevalent glacial and deglaciation conditions.

The core (5.4 m) was retrieved during the 31st expedition of ORV *Sagar Kanya* (location 15°52′00″N; 91°10′00″E, water depth 2713 m; Figure 1). The upper 100 cm of the core was sub-sampled at 2 cm intervals. Washed, salt-free and oven-dried samples were used for the analyses. d^{18}O $\{[(^{18}\text{O}/^{16}\text{O})\ \text{sample}/(^{18}\text{O}/^{16}\text{O})\text{standard} - 1]10^3\}$ was determined in 25–30 shells (size 315–400 μm, ultrasonically cleaned) of *Globigerinoides sacculifer* and *Globigerinoides ruber* versus PDB standard on a VG Micromass Analyser in the isotope laboratory at the University of Kiel. The results have a standard deviation of 0.04‰.

The salt-free, oven-dried samples were subjected to granulometric studies at 1 j intervals[9]. Clay mineral analysis was undertaken on oriented, carbonate and organic carbon free, < 2 μm fractions on a Philips X-ray diffractometer (model PW 1840). Clays have been identified and quantified using the methods of Biscay[10], and Sirocko and Lange[4]. The core was ^{14}C dated (bulk sample) at 10 levels (Table 1). The ^{14}C dates are corrected for global mean sea water age (400 yr) to account for reservoir effects[11].

Twenty-five discrete, air-dried samples of the core were packed into 8 cm^3 styren cubic pots and the magnetic parameters were measured.

Low frequency, X_{lf}, (0.47 kHz) and high frequency, X_{hf}, (4.7 kHz) magnetic susceptibilities were measured on all dried, discrete samples with a Bartington MS-2 susceptibility meter and mass specific values are presented in 10^{-8} m^3/kg. The frequency-dependent susceptibility (X_{fd}%) was determined using the low and high frequency susceptibilities with a formula[12]: $X_{\mathrm{fd}}\% = (X_{\mathrm{lf}} - X_{\mathrm{hf}})/X_{\mathrm{lf}} \times 100$ to detect the presence of superparamagnetic, ferrimagnetic (magnetite or maghaemite) grains[13,14] of > 0.02 μm. Anhysteretic remanent magnetization (ARM) was imparted on the samples by superposing a DC biasing field of 0.05 mT on a smoothly decreasing alternating field with a peak of 100 mT. All remanences were measured using a Minispin fluxgate spinner magnetometer. Isothermal remanent magnetizations (IRM) acquisations were carried out on a Molspin pulse magnetizer. 'Saturation' isothermal remanent magnetization (SIRM) was imparted using a maximum field of 1 T. After acquisition of SIRM, the samples were subjected to reverse DC fields of 0.3 T, and the remanence was measured using the Molspin magneto-

Table 1. Age model for core (source Chauhan[31])

Laboratory no	Sample interval (cm)	^{14}C age (years)	Corrected ^{14}C age (years)
PRL 1686	0–5	1480 ± 120	1080
KL 31/11-3	4–6	1830 ± 120	1430
KL 31/11-8	14–16	4660 ± 100	4260
KL 31/11-10	18–20	5530 ± 160	5130
PRL 1687	25–30	8860 ± 120	8460
KL 31/11-16	32–34	10300 ± 340–330	9900
KL 31/11-22	44–46	11300 ± 350	10900
KL 31/11 -28	62–64	12300 ± 440–410	11900
KL 31/11-30	68–70	12900 ± 440–410	12500
KL 31/11-35	78–80	15300 ± 500–440	14900

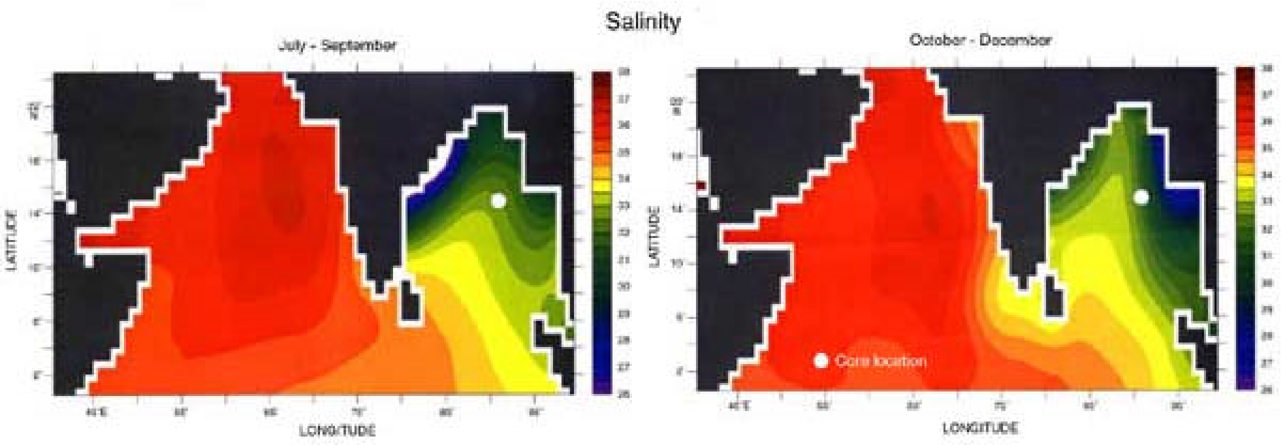

Figure 1. Study area and location of core in the bay. Sea surface salinity variations during the SW (left panel) and NE (right panel) monsoons are shown.

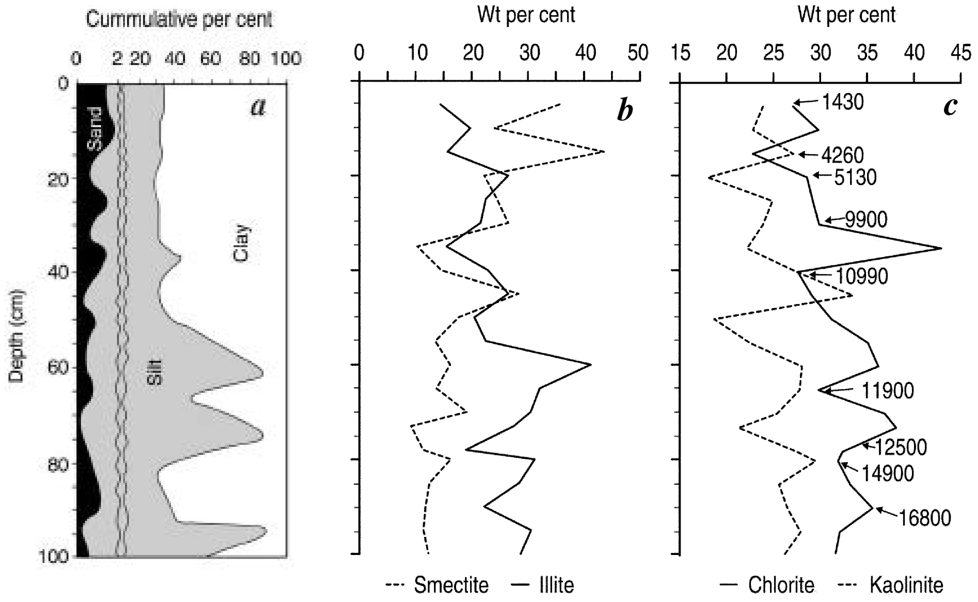

Figure 2. Temporal variations in granulometric parameters and clay minerals in the core. Note enhanced silt and chlorite during arid events. Corrected ages of core levels are also shown.

meter. To investigate the magnetic mineral composition, HIRM (hard IRM) and *S*-ratio ($S_{-0.3}$ T) were calculated using the definitions of Robinson[15] and Bloemendal *et al.*[16].

$$\text{HIRM} = (\text{IRM}_{1\text{T}} + \text{IRM}_{-0.3\text{T}})/2,$$

$$S\text{-ratio\%} = ((1 - \text{IRM}_{-0.3\text{T}}/\text{IRM}_{1\text{T}})/2)*100.$$

HIRM represents the concentration of high-coercivity magnetic minerals such as hematite and goethite. *S*-ratio, however, indicates the proportion of SIRM carried by the low-coercivity component.

The granulometric data of the core are presented in Figure 2. The core can be broadly divided in two sections. In the upper 32 cm levels, < 4 μm size (clay size) detritus is uniformly higher. Below this section, the clay size is reduced, but the silt contents (size range 45–4 μm) are found to be enhanced conspicuously at 36, 65 and 72 cm levels (Figure 2). Illite, chlorite, smectite and kaolinite are the significant clays present (Figure 2). Abundance of chlorite and illite shows an inverse trend; chlorite being more abundant at 82–100 (15–20 Ka BP), 72 (12.7 Ka BP), 36 (10.5 Ka BP), 18 (4.5 Ka BP) and 8 cm (~ 2.1 Ka BP) levels.

d^{18}O variations in the core are presented in Figure 3. Broadly, derived from the heavier synchronous incursion of d^{18}O in both the planktonic species, we infer reduced fluvial influx due to enhanced glaciation during 15–20, 12.7,

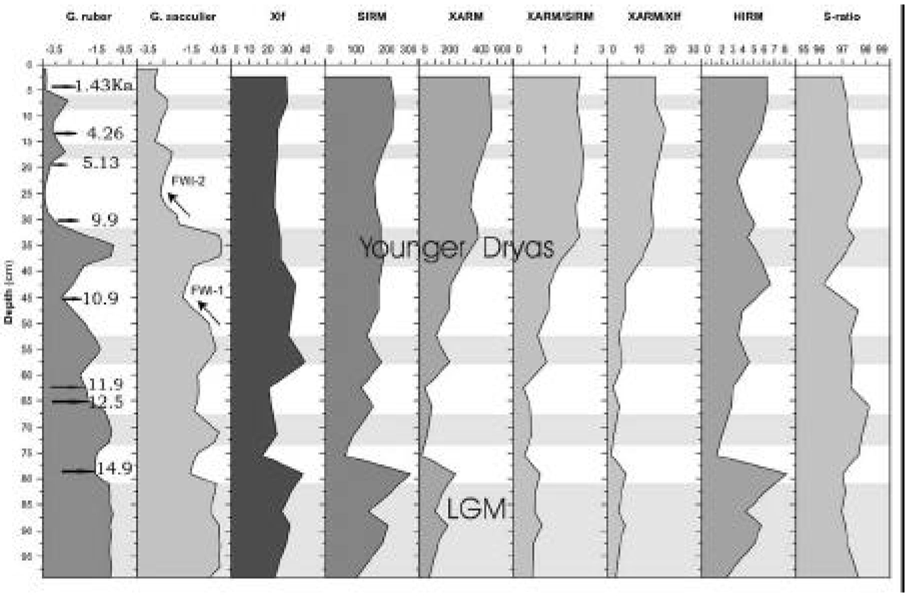

Figure 3. Temporal variations in magnetic parameters and d^{18}O (‰PDB) in *G. ruber* and *G. sacculifer* in the core. Major glaciation events are schematically shown in grey shades. Events of Fluvial Water Influx (FWI) I and II are shown by thick arrows.

10.5, ~ 5–4.3 and 2.2–1.8 Ka BP. The events of 20–15 and 10.5 Ka BP are coeval with global glaciation events of Last Glacial Maximum (LGM) and Younger Dryas (YD)[17]. Other glaciation events of 12.7, ~ 5–4.3 and 2.2–1.8 Ka BP have also been reported in continental and marine records[17–32]. We have observed significant lighter incursions after 11.5 and 9.5 Ka BP.

The X_{lf} and SIRM variations in the core are marginal with average values of 27.78×10^{-8} m^3/kg and 169.28×10^{-8} m^3/kg respectively. However, these two parameters, representing ferromagnetic contents in the samples, match well with the isotope variations during pre-Holocene section of core (38–100 cm). From these indices, a relatively higher ferromagnetic component is deduced during the arid, glacial events characterized by heavier d^{18}O values of *G. ruber* and *G. sacculifer*. In order to further understand the grain size-specific variations in the magnetic parameters, we have determined ratio parameters, susceptibility of anhysteretic remanant magnetism (XARM)/SIRM, XARM/X_{lf} (Figure 3). Finer magnetic grain size, interpreted from the higher, uniform XARM/SIRM ratio, is observed in the entire Holocene section of the core. Below these levels, from the reduced ratios during all arid events, particularly at 35, 65 and 72 cm sections, however, we deduce occurrence of coarser magnetic grain size. These interpretations are also reflected in the granulometric parameters – enhanced silt contents are observed at these core levels.

d^{18}O of foraminifers is reported to be influenced by SSS and SST changes[8]. The core has about 2.44‰ changes in d^{18}O between LGM and Holocene. A change of 1.2‰ is attributed to global climate variability[22,23]. The excess lighter values may, therefore, be attributed to local factors. The estimated temperature variations are 2°C between Holocene and LGM[33–35], which can account only for 0.6‰ variability in d^{18}O. Because temperature variability cannot fully account for the excess lighter d^{18}O values in both the species, the bay being the depocentre of large fluvial influx, these excessive lighter incursions appear to be related with the magnitude of fluvial influx into the bay. The core location lies in the region where the SSS is mostly regulated by climate-regulated fluvial influx of the G–B[1,5,36,37] (Figure 1), with least contributions either from peninsular India or Myanmar sources[1,5]. It may be inferred, therefore, that the d^{18}O variability at the core site is regulated by the magnitude of the fluvial influx from the G–B.

Broadly, derived from the heavier synchronous incursion of d^{18}O in the core, we infer overall elevated SSS and a reduced fluvial influx due to enhanced glaciation during 15–20 12.7, 10.5, ~ 4.8 and 2.2 Ka BP. The Himalayas were intensely glaciated during 20–15, 12.7 and ~ 10.5 Ka BP. These stadials are coeval with global glaciation events[19,26,31,32]. Moreover, from the abrupt large coeval temporal variations in the d^{18}O between 15 and 12.5 Ka BP in both the species, we infer a highly variable magnitude of fluvial influx into the bay till 12.7 Ka BP. This implies that the monsoon regime was highly unstable and the fluvial influx into the bay was unstable after last glaciations until 12.7 Ka BP.

We have observed two major lighter incursions of d^{18}O after 12.7 Ka BP, culminating after 11.5 and 9.5 Ka BP, with the magnitude of 1.88 and 2.44‰ respectively, later being more or less stable in the entire Holocene. As discussed earlier, these lighter incursions, if induced by local temperature alone, shall require about 5–6° SST changes[3], which are much larger than those reported for these times from the bay[33–35]. Therefore, we interpreted these as an evidence of a large reduction (5–6‰) in the SSS. Being the depocentre of major rivers, the SSS in the bay is regulated by the precipitation-regulated magnitude of their influx. At the core site, the G–B system is the most important contributor for SSS variations, irrespective of prevalent hydrography, either during the SW monsoon (anticyclonic, polewards) or the rest of the year (equatorwards, western boundary currents)[1,5,36,37]. We, therefore, infer at least two major episodes of Fluvial Water Influx (FWI) culminating sometime after 11.5 and 9.5 Ka BP. The upper reaches of the Himalayas experienced major deglaciation coupled with humid Tibet during these times[26,32], and this may have augmented the fluvial influx of the Himalayan rivers. These events are also coeval with melt water pulses 1A and IB observed in sea-level records in which global sea-level had risen by 24 and 28 m respectively[17]. We, therefore, suggest that the Himalayan deglaciation also responded to the then prevalent global climate variability. Subsequent to the later pulse, d^{18}O have rather little temporal variability until ~ 5–4.3 Ka BP. Here, deduced from the heavier d^{18}O incursion of 0.3‰, we interpret a reversal in Holocene deglaciation and associated reduction in the magnitude of the fluvial flux. At this time, the Himalayas experienced glaciation (Shivling glaciation[29]) and enhanced aridity at Dokriani glacier[30], which appeared to have influenced the fluvial flux of the Himalayan rivers *vis-à-vis* salinity in the bay. The climate records from the Ganga Plain[38], derived from a core at the Sanai Lake, have aridity between 5000 and 2000 calendar year, which is rather prolonged than observed in our study. This prolonged arid event, however, appeared to have stemmed from the limitation of sampling resolution due to slow rate of sedimentation and larger sampling intervals during this episode. The other heavier incursion at 1.8–2.1 Ka BP is coeval with the reduction in influx of the Indus, during this time[21,23] related with a pause in the deglaciation of the Himalayas. Coeval with our climatic reconstruction, other studies[27,29–33,38] have also shown a weak SW monsoon (and glaciation at Himalayas) from the continental, lake records as well as marine records at these times during mid–late Holocene.

The supply of clays from a source depends upon geology, drainage and climate of the region. For a short geologic time span of the 20 Ka, it may be deduced that the geology had rather insignificant variations. Also, from the soil-profile studies along the different climate zones[39], it is established that augmented chlorite is produced under arid, cold climate due to higher magnitude of physical weathering. With increase in the precipitation, production of smectite–illite–kaolinite–gibbsite in the increasing order is observed[35]. In the bay, derived from the load of the rivers, it is deduced that illite, chlorite with minor kaolinite are found in the suspended sediments of the G–B system[40]. Smectite, the clay conspicuous by its absence in the load of the G–B system, is the major constituent of rivers draining the Deccan Basalt in the central peninsular India[23]. From the temporal variations in the clays in the bay[27], it is also deduced that chlorite contents, inversely related with illite, are enhanced during glacial events due to enhanced physical weathering with corresponding reduction in illite. Temporal variations in the clay assemblage of the G–B system, therefore, have potential to be used as a proxy to reconstruct weathering intensity in the hinterland.

The abundance of clays in the core varies significantly. Chlorite is a dominant clay species during the entire pre-Holocene. The augmented content of chlorite during all the arid events of 20–15, 12.7, 10.5, 5–4.8 and 2.1–1.8 Ka BP, and the corresponding decrease in illite (Figure 2) appeared to stem from the intensified physical weathering at the glaciated Himalayas. The contents of enhanced illite *vis-à-vis* reduced chlorite during deglaciation events, particularly during the Holocene and the events of FWI (Figure 2) also suggest higher component of chemical weathering in the Himalayas under intensified precipitation regime. The temporal variability in the content of the silt in the core, being coeval with chlorite – the clays reported to have enhanced production under intensified glaciation, further support our view of enhanced physical weathering in the Himalayas during stadials.

The magnetic properties of the sediments stem from composition, concentration and grain size of the magnetic minerals, and are therefore related with changes in sources, climatically influenced concentration and grain size regulated by changes in transport processes, e.g. turbiditic, bottom currents, fluvial input, eolian, melt water and ice rafting[13–15]. The core being turbidity-free, and located in hemipelagic environment[6], suspension is the prominent mode of deposition. X_{lf} variations in the core are the least. Low X_{lf} values (Figure 3) further imply that the core site is not an active depocentre of magnetic material. This is expected since the core location lies far away from the continental margins, and the mouths of the major fluvial sources in the bay. Also, in the bay, the fluvial input is the only major source. The sediments have rather low hard component (around 3%), which is attributed to an insignificant presence of hematite component. *S*-ratio associated with the occurrence of titanomagnetite is significantly high (~ 97.34%). Considering the high values of *S*-ratio, we infer that titanomagnetite is the only major constituent of the sediments. Titanomagnetite has major sources in volcanic, acid igneous and metamorphic rocks[41]. In the bay there are two potential sources – (i) from the Deccan Basalt and (ii) from the Sylhet Basalt in the catchment of the G–B system[41]. To the core sites, magnetic material can be contributed either through bed load or advection in suspension. The contribution of titanomagnetite from peninsular India appears unlikely because it cannot be transported in bed load for several hundred km across the bay, escaping entrapment within the channel levees system of middle fan regions having physiographic modulation of about 100 m. Its advection in suspension is also unlikely because of the hydrography of the bay. The anticyclonic poleward currents prevalent during the SW monsoon[1,5,36,37] advect the discharge of the Krishna and the Godavari rivers, the major source of titanomagnetite, northwards, and not across 10°E at the same latitude. The hydrography during the rest of the year is mostly cyclonic, western boundary currents (equatorwards), which also advect suspended load southwards[1,36–37,42]. Therefore, the supply of titanomagnetite from the Deccan Basalt appears unlikely. This implies that the magnetic material has been mostly supplied from the Himalayan source. Other studies have also identified titanomagnetite as the main magnetic carrier contributed from the Himalayas in the central regions of the bay[41]. Considering supply of magnetic material from a single source and uniform mode of deposition, the temporal variations in the magnetic grain size appear related with climatic changes.

We have consistently found reduced ARM/SIRM ratio during the LGM and YD periods compared to the Holocene – the period with intensified precipitation regime. We have observed enhanced influx of silt size detritus during the glacial events at 36 and 72 cm levels coeval with chlorite (Figure 2). We link this with: (i) a reduced chemical weathering in the hinterland aiding in the augmented supply of coarser material; (ii) change in the land vegetation pattern (reduced during weak precipitation) aiding in contribution of coarser sediments, and (iii) location of the mouth of the fluvial sources farther offshore at the edge of the continental shelf due to about – 120 m low stand of sea[8,17]. A proximal location of the river mouth during the low stand of sea level has been found to induce an enhanced terrigenous flux into the bay[25], and further supports our thesis. A higher ARM/SIRM ratio, coupled with high (low) clays (silt) fraction, similarly, may also be attributed to higher intensity of chemical (physical) weathering and augmented influx of finer magnetic grain from the catchment area under intensified monsoon regime during the entire Holocene.

It is summarized that climate variability has influenced the characteristics of terrigenous influx. During glaciation events, under the intensified regime of physical weathering, there was an enhanced flux of coarser material, which has reduced considerably under intensified monsoon regime during the Holocene.

---

1. Varkey, M. J., Murthy, V. S. N. and Suryanarayana, A., Physical oceanography of the Bay of Bengal and Andaman Sea. *Oceanogr. Mar. Biol.*, 1996, **34**, 1–70.
2. Webster, P. J., The elementary monsoon. In *Monsoon* (eds Fein, J. S. and Stephens, P. L.), Wiley, New York, 1987, pp. 3–32.
3. Sarkar, A., Ramesh, R., Bhattacharya, S. K. and Rajagopalan, G., Oxygen isotope evidence for a stronger winter monsoon current during the last glaciation. *Nature*, 1990, **343**, 549–551.
4. Sirocko, F. and Lange, H., Clay mineral accumulation rates in the Arabian Sea during Late Quaternary. *Mar. Geol.*, 1991, **97**, 105–119.
5. Levitius, S., Burgett, R. and Boyer, T. P., In *World Ocean Atlas* Salinity NOAA Atlas NESDIS 3, US Department of Commerce, Washington DC, 1994, vol. 3.
6. Kolla, V. and Rao, N. M., Sedimentary sources in surface and near surface sediments of the Bay of Bengal. *Geo-Mar. Lett.*, 1991, **10**, 125–136.
7. Chauhan, O. S., Borole, D. V., Gujar, A. R., Antonio, M., Mislanker, P. G. and Rao, C. H. M., Late Quaternary sedimentation in eastern Bay of Bengal. *Curr. Sci.*, 1993, **65**, 558–562.
8. Duplessy, J. C., Glacial to interglacial contrast in the northern Indian Ocean. *Nature*, 1982, **295**, 494–498.
9. Folk, R. L., A review of grain size parameters. *Sedimentology*, 1966, **6**, 73–98.
10. Biscay, P. E., Mineralogy and sedimentation of recent deep-sea clays in the Atlantic Ocean and adjacent seas and oceans. *Bull. Geol. Soc. Am.*, 1965, **76**, 803–832.
11. Stuiver, M. and Reimer, P. J., Extended ^{14}C data base and revised calibration 3.0 ^{14}C age calibration programme. *Radiocarbon*, 1993, **35**, 215–230.
12. Mullins, C. E. and Tite, M. S., Magnetic viscosity, qudrature susceptibility and frequency dependence of susceptibility in single-domain assemblies of magnetite and maghemite. *J. Geophys. Res.*, 1973, **78**, 804–809.
13. Bloemendal, J., Barton, C. E. and Radhakrishnamurthy, C., Correlation between Rayleigh loops and frequency dependent and quadrature susceptibility: Application to magnetic granulometry of rocks. *J. Geophys. Res.*, 1985, **90**, 8789–8792.
14. Thompson, R. and Oldfield, F., *Environmental Magnetism*, Allen and Unwin, London, 1986, p. 227.
15. Robinson, S. G., The Late Pleistocene palaeoclimatic record of North Atlantic deep-sea sediments revealed by mineral magnetic measurements. *Phys. Earth Planet. Inter.*, 1986, **42**, 22–47.
16. Bloemendal, J., King, J. W., Hall, F. R. and. Doh, S. J., Rock magnetism of Late Neogene and Pleistocene deep-sea sediments – relationship to sediment source, diagenetic processes and sediment lithology. *J. Geophys. Res.*, 1992, **97**, 4361–4375.
17. Fairbanks, R. G., A 17,000 year glacio-eustatic sea level record: Influence of glacial melting rates on the younger dryas event and deep ocean circulation. *Nature*, 1989, **342**, 637–642.
18. Blanchon, P. and Shaw, J., Reef drowning during the last deglaciation: Evidence for catastrophic sea-level rise and ice-sheet collapse. *Geology*, 1995, **23**, 4–8.
19. Sarkar, A., Ramesh, R., Somayajulu, B. L. K., Agnihotri, R., Jull, A. J. T. and Burr, G. S., High resolution monsoon record from the eastern Arabian Sea. *Earth Planet. Sci. Lett.*, 2000, **177**, 208–218.
20. Dansgard, G. W. *et al.*, Evidence for general instability of past climate from a 250-kyr ice core record. *Nature*, 1993, **364**, 218–220.
21. Von Rad, U., Schaaf, M., Michels, K. H., Schulz, H., Berger, W. H. and Sirocko, F., A 5000 year record of climate change in varved sediments from the oxygen minimum zone off Pakistan northeastern Arabian Sea. *Quat. Res.*, 1999, **51**, 39–53.
22. Sirocko, F., Garbe-Schonberg, D., McIntyre, A. and Molfino, B., Teleconnection between the subtropical monsoon and high-latitude climate during the last deglaciation. *Science*, 1996, **272**, 526–529.
23. Chauhan, O. S., Sukhija, B. S., Gujar, A. R., Nagabhushanam, N. and Paropkari, A. L., Later quaternary variations in clay mineral along the SW continental margin of India: evidence of climataic variation. *Geo.-Mar. Lett.*, 2000, **20**, 118–122.
24. Johnson, T. C. *et al.*, Late Pleistocene desiccation of Lake Victoria and rapid evolution of cichlid fishes. *Science*, 1996, **273**, 1091–1093.
25. Weber, M. E., Wiedicke, H. M., Kudrass, H. R., Hubscher, C. and Erlenkeuser, H., Active growth of the Bengal Fan during sea-level rise and highstand. *Geology*, 1997, **25**, 315–318.
26. Phardtare. N. R., International Conference on Quaternary Climate, Tectonics and Environment of the Himalaya: Comparison with other Regions, Nainital, 2002, pp. 16–17.
27. Chauhan, O. S. and Suneethi, J., 18 ka BP records of climatic changes, Bay of Bengal: Isotopic and sedimentological evidences. *Curr. Sci.*, 2001, **81**, 1231–1234.

28. Duplessy, J. C., Delibrias, G., Turon, J. L., Pujol, C. and Duprat, J., De glacial warming of the northeastern Atlantic Ocean: correlation with the palaeoclimatic evolution of the European continent. *Paleogeogr. Paleoclimatol. Palaeoecol.*, 1981, **35**, 121–144.
29. Sharma, M. and Owen, L. A., Quaternary glacial history of the Garhwal Himalayas, India. *Quat. Sci. Rev.*, 1996, **15**, 335–365.
30. Phadtare, N. R., Sharp decrease in summer monsoon strength 4000–3500 cal yr BP in the central higher Himalays of India based on pollen evidences from alpine peat. *Quat. Res.*, 2000, **53**, 122–129.
31. Chauhan, O. S., Past 20,000-year history of Himalayan aridity: Evidenced from oxygen isotope records in the Bay of Bengal. *Curr. Sci*., 2003, **84**, 90–93.
32. Sharma, C., Chauhan, M. S., Gupta, A. and Rajagopalan, G., Vegetation and climate of Garhwal Himalayas during last 4000 years BP. In Symposium on Recent Advances in Geological Studies of Northwest Himalaya and Foredeep, Geological Survey of India, Lucknow, 1995, abstr. vol., p. 90.
33. Rostek, F., Bard, E., Beafort, L., Sonzogni, C. and Ganssen, G., Sea surface temperature and productivity records for the past 240 kyr in the Arabian Sea. *Deep-Sea Res. II*, 1997, **44**, 1461–1480.
34. Sonzogni, C., Bard, E. and Rostek, F., Tropical sea-surface temperatures during the last glacial period: a view based on alkenones in Indian Ocean sediments. *Quat. Sci. Rev.*, 1998, **17**, 1185–1201.
35. Kudraas, H. R., Hofman, A., Doose, H., Emeis, K. and Erlenkueser, H., Modulation and amplification of climate changes in Northern Hemisphere by Indian summer monsoon during the past 80 ky. *Geology*, 2001, **29**, 63–66.
36. Shetye, S. R., Shenoi, S. S. C., Gouveia, A. D., Michael, G. S., Sundar, D. and Nampoothri, G., Wind driven coastal upwelling along the western boundary of the bay of Bengal during southwest monsoon. *Continental Shelf Res*., 1991, **11**, 1397–1408.
37. Shetye, S. R., Gouveia, A. D., Shenoi, S. S. C., Sundar, D., Michael, G. S. and Nampoothri, G., The western boundary current in the seasonal subtropical gyre in the Bay of Bengal. *J. Geophys. Res*., 1993, **98**, 945–954.
38. Sharma, S. *et al*., Late glacial and Holocene environmental changes in Ganga plain, Northern India. *Quat. Sci. Rev.*, 2004, **23**, 145–159.
39. Weaver, C. E., *Clays, Muds and Shales*, Elsevier, Amsterdam, 1989, p. 819.
40. Konta, J., In *Mineralogy and Chemical Maturity of Suspended Matter in Major Rivers Samples under SCOPE/UNEP, Transport of Carbon and Minerals in Major World Rivers. Part III* (eds Degens, T. and Kempe, S.), Mitteilungen aus dem Geologisch – Paleontologischen Institut der Universitat Hamburg, 1985, p. 569.
41. Collins, C., Turpin, J., Betaux, A., Desparairies, C. and Kissel, C., Erosional history of the Himalayan and Burman range during the last two glacial–interglacial cycles. *Earth Planet. Sci. Lett*., 1999, **171**, 647–660.
42. Chauhan, O. S., Rajawat, A. S., Pradhan, Y., Suneethi, J. and Nayak, S. R., Weekly observations on dispersal and sink pathways of the terrigenous flux of the Ganga–Brahmaputra in the Bay of Bengal during NE monsoon. *Deep-Sea Res. II*, 2004, in press.

ACKNOWLEDGEMENTS. We thank the Directors of NIO and IIG for providing facilities. We thank M. Sarnthein and E. Vogelsang, University of Kiel for carbon and oxygen isotopic analysis and interpretation. This is NIO contribution no. 3890.

Received 17 January 2004; revised accepted 28 April 2004

Seismic reflection data: their utility in estimation of gas hydrates in deep marine sediments

Uma Shankar, N. Satyavani, Babita Sinha and N. K. Thakur*

National Geophysical Research Institute, Uppal Road,
Hyderabad 500 007, India

The occurrence and significance of low-velocity sedimentary layer corresponding to free gas in the sediment beneath the bottom simulating reflector have long been a subject of debate. Either velocity or amplitude information in isolation is inadequate to estimate hydrate concentration. Reduction in amplitude (amplitude blanking) calibrated by interval velocity has been used to quantify hydrate concentration in the Kerala–Konkan area of western continental margin of India. The tentative estimate of hydrate in the representative sediment has been made using the time-average equation, in which the velocity structure of pure methane hydrate is inferred from the seismic data and known properties of pure hydrate.

A bottom simulating reflection (BSR) at a depth corresponding approximately to the base of the methane hydrate stability field is the most widely used indicator for the probable presence of gas hydrate accumulations beneath the sea bed. BSRs are observed worldwide on reflection seismic data from continental margins[1,2]. Models have been developed to estimate the amount of hydrate or free gas associated with BSR[3–6]. Only few of these models are constrained by independent drilling or laboratory data. An important indicator of the gas hydrates is the amplitude reduction or blanking observed above the BSR in seismic reflection profiles from the region of known hydrates. The marked decrease in amplitude above the BSR was related to a reduction in impedance contrast across sedimentary interfaces caused by the presence of hydrates[7,8].

Seismic reflection data suggest that an extensive accumulation of gas hydrate underlies the western continental margin of India (WCMI) in the Kerala–Konkan basin[9]. These gas hydrate accumulations are inferred from the presence of a BSR that lies 400 ms two-way travel time (TWT) beneath the seafloor (Figure 1). This depth closely approximates the base of the methane hydrate stability field[9], indicating that this strong reflection event marks the base of hydrate-bearing sediments. The high reflection amplitude and reverse reflection polarity of the BSR with respect to the sea floor reflection allow us to infer the base of the hydrate.

Two types of analysis have been undertaken in this study: (i) Analysis of the BSR reflection amplitude and the nature of the BSR, and the inference of hydrate layer

---

*For correspondence. (e-mail: nkthakur@ngri.res.in)